Reaction Kinetics, Mechanisms and Catalysis (2021) 134:221–242
https://doi.org/10.1007/s11144-021-02048-y

Oxidation of soot over supported RuRe nanoparticles prepared by the microwave-polyol method

Katarzyna Adamska[1] · Szymon Smykała[2] · Sebastian Zieliński[3] · Damian Szymański[1] · Agnieszka Hojeńska[1] · Paweł Stelmachowski[3] · Andrzej Kotarba[3] · Janina Okal[1]

Received: 8 June 2021 / Accepted: 31 July 2021 / Published online: 7 September 2021

Abstract

The oxidation of soot over RuRe bimetallic nanoparticles (NPs) supported on γ-Al_2O_3 has been investigated. The catalysts were synthesized by a microwave-polyol method and characterized by ICP, BET, TEM, STEM-EDS, XRD and XPS techniques. The study revealed that the proper choice of the Re loading (0.4–2.0 wt%) is crucial for the catalytic behavior of the 2% Ru–Re/Al_2O_3 nano-catalysts.The best catalytic properties, in terms of overall activity and stability, were observed for the 2%Ru-0.8%Re/γ-Al_2O_3 nano-catalyst. The stability of all bimetallic 2% Ru–Re nano-catalysts in catalytic soot oxidation in the presence of oxygen is very high in contrast to the 2% Ru/γ-Al_2O_3 sample. The presence of rhenium in the catalytic system hinder the formation of large RuO_2 agglomerates leading to a better dispersion of active ruthenium phase and a better catalytic performance. The relationship between the catalytic activity of Ru–Re/γ-Al_2O_3 and the synergetic roles of Ru and Re is discussed.

Keywords Bimetallic catalysts · RuRe nano-catalysts · Soot oxidation · High stability

✉ Janina Okal
J.Okal@intibs.pl

[1] Institute of Low Temperature and Structure Research, Polish Academy of Sciences,, Okólna 2, 52-422 Wrocław, Poland

[2] Department of Engineering Materials and Biomaterials, Faculty of Mechanical Engineering, Silesian University of Technology, Konarskiego 18a, 44-100 Gliwice, Poland

[3] Faculty of Chemistry, Jagiellonian University, Gronostajowa 2, 30-387 Kraków, Poland

Introduction

Particle matters (PM) suspended in the air are responsible for the black smoke, which is one of the biggest problems of modern society. The main source of harmful particulate matters are car engines, especially diesel engines. The gasoline direct injection engines can easily comply with the PM gravimetric Euro 6 limit, but solid particles emitted from them are very small (mostly below 100 nm) and particulate number (PN) emission significantly exceeds the acceptable threshold [1]. For this reason, the newest EU regulations enforce the control of the particulate emission also from gasoline engines. Particle matters with diameters below 10 μm can be present in the air for a long time and are recognized as the most harmful particles for human bodies. A high concentration of $PM_{2.5}$ in the air has been linked to increased morbidity and mortality because they can penetrate the lungs causing asthma, chronic obstructive pulmonary disease, and atherosclerosis [2]. However, the diesel and gasoline particulate matters consist not only of carbonaceous soot but also minor components of the volatile organic fraction (VOF) from unburned fuel, lubricating oil, and inorganic phases, for example, ash or sulfur combinations [3]. Several of these compounds are considered carcinogenic and mutagenic.

So far particulate filters are considered as the only efficient solution for lowering the PM emissions from cars [4]. However, the removal of the soot accumulated on the filter pores is required in order to prevent the clogging, building up a back-pressure and consequently the destruction of the filtering system. The process of trapped PM oxidation by O_2 molecule can be performed when a pre-determined quantity of soot is collected [5, 6]. The additional portion of fuel needs to be injected into the hot exhaust for rising the adiabatic temperature and consequently, the catalytic combustion of the soot within the filter can occur.

Various forms of catalysts were proposed for lowering the soot oxidation temperature. The noble metal-based systems (Pt, Pd, Rh) are mostly used in the automotive exhaust control catalysts because of their high activity and stability. Limited availability and the high cost of platinum and palladium have been a reason for the search for alternative catalysts. Cerium or iron-based catalysts can be used as fuel additives that embed into the soot structure and lower the ignition temperature of PM [7]. On the other hand, non-noble metals oxides like Ni, Co, Cu, Mn are not durable for automotive applications, because of their intrinsic reactivity and lack of resistance to poisoning [8].

New catalytic systems are still under development. The main issues are: lowering the filter's regeneration temperatures, decreasing the cost of the catalysts, and improving their effectiveness. A large portion of the particulate matters produced by realistic combustion engines includes porous soot within which organic molecules can be condensed and adsorbed [9]. As the engine exhaust cools, these molecules may pass from the gas phase to create fine particulate matters [10]. The condensed or adsorbed hydrocarbons molecules can be up to 25% by a soot mass and act as precursors of the elemental carbon within the particles [9, 11]. Although a lot of studied catalytic systems were proved to be active in the

combustion of elemental carbon they are not good enough to remove the condensed toxic molecules from the engine's exhaust. Due to this fact, it is rational to search for a new catalytic system, stable and active in both hydrocarbon and soot combustion.

Ruthenium is a very active catalyst in important reactions for industry, such as ammonia synthesis [12] or the Fischer–Tropsch process [13]. Recently, much attention has been devoted to research on the use of ruthenium in oxidation reactions of, e.g.: ammonia [14], alcohols [15] or carbon monoxide [16]. The Ru/Al_2O_3 catalyst also exhibits the capacity to strong chemisorption of the naphthalene and activity in the total oxidation of this molecule [17]. In a previous study we also shown that Ru/Al_2O_3 [18] and Ru/CeO_2 [19] are highly efficient catalysts for oxidation of the light alkanes (C_1–C_4). More recently, a few studies have been devoted to the oxidation of soot in the presence of Ru-based catalyst [20–24]. Ruthenium supported on zeolite is active in the oxidation of carbon particles by NO_2, which is a stronger soot oxidant than oxygen [22]. On the other hand, Villani et al. found that in the absence of NO_x, the Ru/Na-Y catalyst catalyzes the soot oxidation at temperatures about 100 °C lower than the Pt/Na-Y catalyst [23]. Hence, the authors claimed that unlike platinum catalysts, carbon oxidation by a zeolite-supported ruthenium catalyst does not require the presence of NO_x in the gas stream and this catalyst opens up a new route for catalytic soot oxidation in diesel engine exhaust filters. A comparison between ruthenium and platinum based catalysts in C–O_2 and C–NO_2 showed that Ru catalysts are more active in both types of reactions compared to Pt based catalyst [24]. However, during the soot combustion reaction progressive conversion of the Ru into the bulk RuO_2 oxide occurred and it is a reason for deactivation of the ruthenium catalyst [23]. Additionally, one of the factors that Ru is not used as the automotive catalyst instead of Pt and Pd is that it forms volatile oxides at high temperatures [8]. Villani et al. studied the stability of Ru/zeolite-based catalysts and found 900 °C as the upper limit temperature for practical applications of Ru-based catalysts [23]. Several studies were carried out at Ford company to improve the Ru stability against volatilization, e.g. by deploying it in the form of various ruthenate compounds like $BaRuO_3$, $SrRuO_3$, or $LaNi_xRu_{1-x}O_3$ but the ruthenium in that state loses its excellent catalytic properties in soot oxidation [8].

The solution to the problem of the low thermal stability of the ruthenium may be the introduction of a second metal into the system and the application of new techniques for the preparation of the metallic particles. The polyol reduction method, in which the polyol acts both as a solvent of the metal salt and as reducing agent, is one of the most effective for this purpose. It was found that the Ru/TiO_2 catalyst prepared by this method and used for partial oxidation of methane, demonstrates a much stronger metal-support interaction and a following higher thermal stability than an analogical sample prepared by traditional impregnation method [25]. In our previous work, we reported that colloidal synthesis in ethylene glycol using a microwave reactor is an effective new method for obtaining RuRe bimetallic nanoparticles (NPs) with the diameters of a few nanometers [26]. Generally bimetallic catalysts are mostly prepared by co-impregnation or sequential impregnation methods. However, these methods frequently lead to ill-defined morphologies of the supported bimetallic catalysts and an uneven distribution of active sites. An improved

method to achieve higher uniformity of the bimetallic catalysts, in which the two metals are bonded to each other are the polyol method or a combined microwave irradiation-polyol method [26]. Additionally, microwave-assisted polyol synthesis of bimetallic NPs represents a sustainable and green approach to the preparation of supported nanostructured catalysts using environmentally friendly and less energy-demanding conditions, compared with those involved in traditional methods. This technique allows very rapid uniform heating of the metal precursors and this shortens the crystallization period of the metal NPs, leading to more homogeneous nucleation when compared to conventional synthesis methods. In this way nanostructures with smaller sizes, narrower size distributions, and a higher degree of crystallization are obtained under microwave (MW) heating. Baranowska and Okal found that the RuRe NPs in situ deposited on γ-Al_2O_3 were very stable, did not tend the agglomeration and their activity in the propane oxidation was higher than that of the Ru nano-catalyst [27, 28]. Generally, rhenium is known as a good promotor for catalytic application causing the improvement of the active phase stability [29]. In the Pt-Re reforming catalyst, the sintering of small-sized nanoparticles (several nanometers and smaller) during the catalytic reaction was significantly inhibited thanks to the presence of Re atoms [30]. The RuRe catalysts are also active and stable in the high-temperature methane oxidation [31], hydrogenation of succinic acid [32], hydrodeoxygenation of lignin [33], and hydrogenolysis of guaiacol [34] or sorbitol [35].

The purpose of this study was to prepare a series of Ru–Re bimetallic nano-catalysts with different atomic ratios (Ru/Re = 9:1, 9:2, 9:3, 9:4 and 9:5) and to investigate the catalysts performances for the soot combustion. Bimetallic RuRe NPs prepared by the colloidal microwave-assisted synthesis were in situ deposited on the γ-Al_2O_3 and next characterized by BET, ICP, TEM, STEM-EDS, XRD and XPS methods. Activity of the catalysts (in the absence of NO_x) was checked using thermogravimetry in the tight contact between soot and catalysts with the ratio soot:catalysts = 1:8 w/w. Despite the high activity of supported Ru catalysts in various oxidation reactions, little research has been done on the possibility of using ruthenium catalysts for the oxidation of solid carbon. To the best of our knowledge, no literature data are available on the use of RuRe nano-catalysts for the soot combustion. It could be noted that the proposed Ru–Re system is cheaper than Pd or Pt-based catalysts. The current price of Ru and Re is about $ 750 and $ 250 per ounce, respectively and they are lower than the Pd ($ 2600 an ounce) and Pt ($ 1100 an ounce).

Experimental

Preparation and treatment of the catalysts

γ-Al_2O_3 support with purity of 99.99% was purchased from US Research Nanomaterials. The microwave-polyol synthesis of RuRe NPs involved the reduction of $RuCl_3 \cdot 3H_2O$ (Alfa Aesar) and NH_4ReO_4 (Alfa Aesar) with ethylene glycol (EG) in the presence of the alumina support. First, the proper amount of the metal precursors was dissolved in 50 ml of EG and stirred magnetically at room

temperature (RT) for 10 h. Next, 10 drops of NH_4OH was added to the solution to achieve pH = 7.5, and in the next stage γ-Al_2O_3 (c.a. 2.7 g) was added to form a suspension. The mixture was magnetically stirred again for 15 min at RT and next put in a Teflon vessel placed in an autoclave with microwave heating (MW Reactor, Ertec, Poland). The synthesis time was set up to 20 min and the reaction proceeded at 190–200 °C under autogenic pressure of 20–23 atm. After the reaction was completed the vessel was rapidly cooled down in an ice-water bath. The suspension was mixed with the 250 ml of the NH_4NO_3 solution (0.3 M), filtered, and washed several times with distilled water to remove the chlorine and others ions. After drying under vacuum at RT, part of the as-prepared sample was treated in hydrogen flow (heating rate 5 °C/min) at 400 °C for 3 h in order to clean the catalyst surface from adsorbed organic species. The same procedure was used to prepare supported Ru NPs. The reduction of the rhenium salt by EG without the presence of ruthenium was not possible. Because of that, we used the wet impregnation method to obtain the reference 0.8% Re/γ-Al_2O_3 catalyst, which after impregnation, drying in air at RT and next at 110 °C (15 h) was reduced in hydrogen flow at 500 °C for 5 h. The samples were stored in a closed containers until using it.

In the bimetallic nano-catalysts, the Ru amount was kept as 2 wt% and the amount of Re was changed: 0.4, 0.8, 1.2, 1.6 and 2.0 wt%. (Ru:Re atomic ratio was 9:1, 9:2 9:3, 9:4 and 9:5, respectively). Additionally, we also decided to synthesize a bimetallic nano-catalyst with a high Ru loading of 5 wt% and Re loading of 2 wt% to be able to observe specific properties of the RuRe NPs. In the samples with a small amount of the active phase—the observations were sometimes impossible because of the detection limit of the measuring equipment.

Catalyst characterization

Ru and Re loadings in the as-prepared samples were measured by the ICP-OES method. Uniformity and chemical composition of the nano-catalysts was confirmed with FE-SEM microscope (FEI NovaNano SEM 230) equipped with EDS analyzer (EDAX Genesis XM4). Elemental distributions and weights were determined by either a point of a user-designed size or of a region within the sample. Textural properties of the samples were estimated by N_2 adsorption–desorption at − 196 °C by using Micrometrics ASAP 2020 C system. Prior to the measurement's samples (0.2 g) were dehydrated in a vacuum at 250 °C for 4 h.

Morphological and structural characterization of the catalysts were performed by transmission electron microscopy (TEM) and high-resolution TEM (HRTEM). HRTEM images were obtained with Philips CM 20 Super-Twin microscope with accelerating voltage of 200 kV providing 0.25 nm resolution. Gatan Digital Micrograph software was used to analyze the results. Additional atomic EDS analysis was performed using STEM TITAN 80–300 microscope equipped with EDAX EDS spectrometer. STEM images were collected with a 24.5-mrad probe semi-angle and recorded by HAADF detector at 47–200 mrad range.

Crystallographic structure and phase composition were determined by X-ray diffraction using PANanalytical X'Pert PRO diffractometer equipped with the copper anode (Cu K_α radiation, $\lambda = 1.5406$ Å).

The X-ray photoelectron spectroscopy (XPS) with the possibility to perform the in-situ thermal treatments in hydrogen was applied to estimate the surface composition and chemical state of the selected samples. The XPS spectra were collected using monochromatized Al source (XM 650 X Ray Monochromator) operating at 360 W and a Scienta R4000 electron analyzer. All measurements were carried out with an electron flood gun source. The pass energy of the analyzer was set at 200 eV for wide-range scan and 50 eV for high resolution spectra. The spectra were collected and curve-fitted by using the CasaXPS software (version 2.3.16 PR 1.6), taking into account the relative sensitivity factors. The spectra were charge corrected (917 eV) and quantified after background (Shirley) subtraction and deconvolution.

Catalytic measurements

Before measuring catalytic activity, the nano-catalysts were heated/activated in air at 500 °C for 1 h. The activity in a soot combustion has been investigated by thermogravimetric measurements in the flow of synthetic air 50 ml/min + Ar 20 ml/min, using Mettler Toledo—TGA/DSC 3 + Thermogravimetric Analyzer with the large furnace (LF). Printex 80 manufactured by Degussa was used as a model soot, which is widely applied as a model substance for diesel particulate. Before catalytic activity evaluation, catalyst-soot mixtures were prepared by grinding the catalyst powder with soot (8:1 on a mass basis) in an agate mortal for 10 min, thus realizing a tight contact. Next, 100 mg of this mixture was loaded in an alumina crucible and heated from RT to 600 °C with a rate of 5 °C/min. For the monometallic Ru and bimetallic RuRe samples, three consecutive cycles were carried out. For the γ-Al_2O_3 and Re/γ-Al_2O_3 catalyst only one cycle was performed to check the Re or catalyst support contribution. From our reproducibility tests, to compare activity between various catalysts, we determined the experimental error of ± 4 °C, for the tight contact in the soot: catalyst ratio used in this investigation.

Results and discussion

Composition and textural results

Table 1 presents nominal and actual Ru and Re loadings in the as-prepared samples and atomic ratios of Ru and Re in the bimetallic nano-catalysts. As can be seen both Ru and Re loadings measured by the ICP-OES method for all the catalysts prepared by the microwave irradiation-polyol method are very close to the theoretical loadings established during the synthesis. Thus, for the bimetallic samples with a Ru content of 2 wt% it will be possible comparison of the influence of Re loading (from 0.4 to 2 wt%) on the chemical and catalytical properties of ruthenium. Only for the 5% Ru-2%Re sample the measured Re loading was higher than expected (~ 3 wt%

Table 1 ICP measurements of Ru and Re loadings in the as-prepared Ru and Ru–Re/γ-Al_2O_3 nano-catalysts prepared by the microwave irradiation-polyol method and N_2 adsorption–desorption data obtained for the samples treated in H_2 at 400 °C and next in air at 500 °C

Catalyst	Ru/Re atomic ratio	Actual metal loading (wt%)		BET surface area (m^2/g)		Mean pore diameter (nm)		Total pore volume (cm^3/g)	
		Ru	Re	H_2	air	H_2	air	H_2	air
γ-Al_2O_3	–	–	–	143	143	18.3	17.8	0.66	0.63
2% Ru	1:0	1.98	–	139	134	18.9	19.0	0.66	0.63
2%Ru-0.4%Re	9:1	1.90	0.41	139	136	18.7	18.1	0.65	0.62
2%Ru-0.8%Re	9:2	1.96	0.81	140	135	18.4	18.3	0.66	0.63
2%Ru-1.2%Re	9:3	2.01	1.24	139	136	18.0	18.3	0.63	0.65
2%Ru-1.6%Re	9:4	2.00	1.64	141	138	18.2	18.7	0.64	0.65
2%Ru-2.0%Re	9:5	1.98	2.03	142	136	19.2	18.9	0.68	0.64
5%Ru	1:0	4.93	–	133	130	18.4	18.7	0.63	0.61
5%Ru-2%Re	9:2	4.95	2.97	134	130	17.5	17.9	0.60	0.58
0.8%Re[a]	0:1	–	n.m	138	135	17.3	17.3	0.60	0.60

[a]Re/γ-Al_2O_3 catalyst prepared by the impregnation method

instead of 2 wt%). The results of the chemical analyses indicate complete reduction of the $RuCl_3$ and NH_4ReO_4 precursors to metallic species during used colloidal synthesis and their in-situ deposition onto the γ-Al_2O_3 support. Previously we found that at higher Ru (5 wt%) and Re loading (up to 9.2 wt%) a small portion of Ru in the $RuCl_3$ and Re in the NH_4ReO_4 was not completely reduced and these species were removed as dissolved Ru and Re species during the $NaNO_3$ treatment and consequent filtration and washing procedure with distilled water [26]. The Ru and Re loadings were also determined for the samples treated in air at high temperature of 500 °C. The ICP results (not presented) showed that the Ru and Re content as well as Ru:Re atomic ratios were close to that of in the as-prepared nano-catalysts, indicating that no noticeable loss of Ru and Re (as volatile RuO_4 or Re_2O_7 oxide) occurred during oxidation treatment at 500 °C.

The textural data for all the nano-catalysts and γ-Al_2O_3 support, based on the N_2 adsorption–desorption isotherms (not presented), are summarized in Table 1. The data were obtained for the samples treated in hydrogen at 400 °C and also after their treatment in air at 500 °C. The γ-Al_2O_3 support before measurement was treated in hot EG in the same way as the catalysts—but without the addition of a metal precursor. Generally, γ-Al_2O_3 and all the samples exhibited type IV isotherms typical of mesoporous materials, and their textural properties were only slightly influenced by composition and treatment procedures. The EG treatment and heating in H_2 at 400 °C of the alumina support nearly did not change its initial BET specific surface area (142 m^2/g), pore volume (0.67 cm^3/g) and pore diameter (18.2 nm). For the H_2 treated bimetallic 2% Ru–Re catalysts the values of BET surface area and pore volume are roughly the same (139–142 m^2/g and 0.64–0.68 cm^3/g, respectively) as for the γ-Al_2O_3. However, at higher Ru loading (5 wt%), both in the mono- and bimetallic nano-catalyst, the BET surface area is lower by ~ 7% indicating that the

metal particles may be localized both inside the pores and on the alumina surface. Treatment of the mono- and bimetallic Ru–Re samples in air at 500 °C leads to a small decrease of the BET surface area (134–138 m^2/g), and the total pore volume (0.58–0.65 cm^3/g). The mean pore diameter for all the Ru-based catalysts is in the narrow range 17–19 nm. Some drop of the BET surface area and total pore volume after air treatment may be related to the partial blockage of pores by the formed RuO_2 particles. The textural data presented in Table 1 suggest that particles of the active phase are placed both in the pores and in an external surface of the alumina support.

Additionally, we confirmed by SEM–EDS analysis that in the fresh as-prepared nan-catalysts as well in the H_2 treated, the metal particles were uniformly distributed on the alumina support surface. After air calcination at 500 °C small agglomeration of particles was observed for all the studied nano-catalysts.

Structure characterization of the nano-catalysts after H2 treatment at 400 °C

The XRD patterns recorded for the Ru NPs and Ru–Re NPs deposited on γ-Al_2O_3 after hydrogen treatment at 400 °C are presented in Fig. 1. All the patterns show diffraction peaks at 2Θ of 37.6°, 45.7°, 62°, and 66.6° corresponding only to the structure of the γ-Al_2O_3 (JCPDS 29-0063). Similar XRD patterns were obtained for the nano-catalysts with high Ru content (5 wt%). This suggests that the formed metal NPs are either amorphous or highly dispersed, with particle sizes below the detection limit of the XRD method. The high dispersion of Ru and Ru–Re NPs was confirmed by TEM observation. Fig. 2 shows representative TEM images and

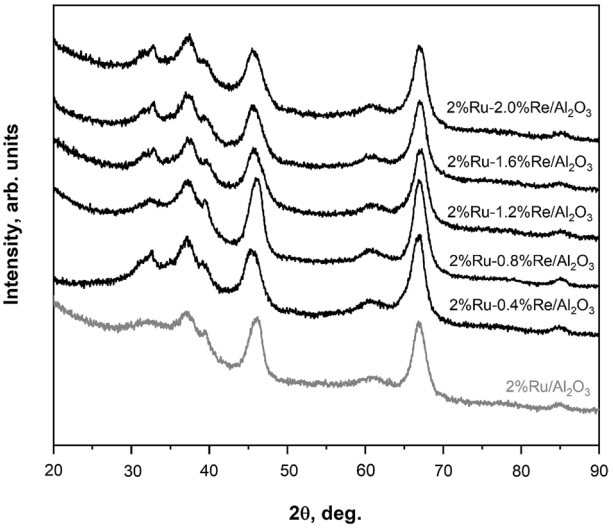

Fig. 1 X-ray diffraction patterns of the monometallic 2% Ru/γ-Al_2O_3 and bimetallic 2% Ru–Re nano-catalysts with different Re content after treatment in H_2 at 400 °C. Peaks from all the patterns are ascribed only to γ-Al_2O_3 structure (JCPDS 29-0063)

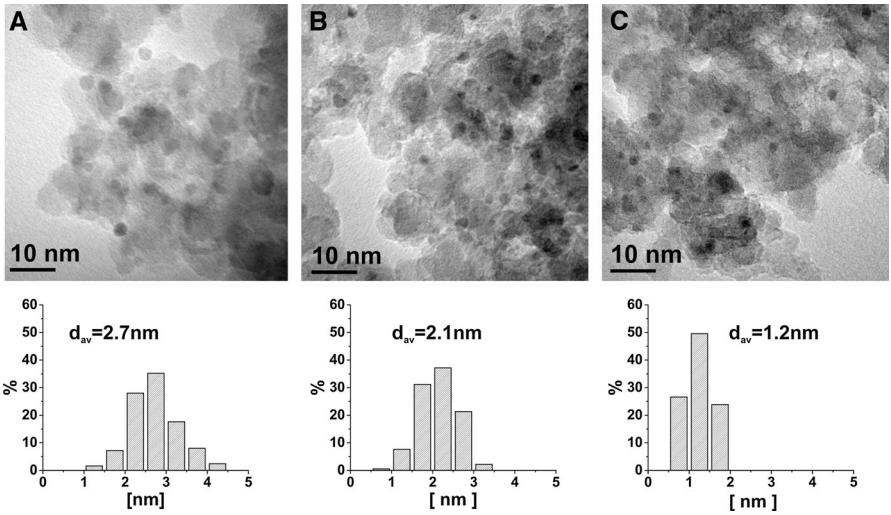

Fig. 2 Representative TEM images and corresponding particle size distributions of the 2% Ru/γ-Al_2O_3 (**A**), 2%Ru-0.8%Re/γ-Al_2O_3 (**B**) and 2%Ru-1.6%Re/γ-Al_2O_3 (**C**) nano-catalysts after treatment in H_2 at 400 °C

corresponding particle size distributions of the 2% Ru and bimetallic 2%Ru-0.8%Re and 2%Ru-1.6%Re nano-catalysts. In all samples we can observe dark dots mainly with a size of 1–3 nm evenly distributed on the alumina support and thus they were undetected by XRD. The mean particle size of the NPs determined from the TEM images amount to 2.7, 2.1 and 1.2 nm for the 2% Ru, 2%Ru-0.8%Re and 2%Ru-1.6%Re nano-catalysts , respectively. Therefore, the monometallic Ru nano-catalyst has slightly larger Ru NPs than both RuRe nano-catalysts. Evidently, Re addition improves the ruthenium dispersion in the bimetallic nano-catalysts, in full agreement with our previous studies performed for the traditionally prepared Ru–Re/γ-Al_2O_3 catalysts (co-impregnation) containing 5 wt% Ru and 1.0–9.2 wt% Re [29]. The high ruthenium dispersion remains unchanged in all bimetallic nano-catalysts even those with high Ru content (5 wt%). Moreover, the range of particle sizes is very narrow in all the synthesized samples.

HAADF-STEM analysis was carried out for sample with high ruthenium and rhenium content (5%Ru-2%Re) since for the catalysts with a less amount of the active phase, it was difficult to perform EDS measurements. The Ru:Re atomic ratio of the 5%Ru-2%Re nano-catalyst is the same as in the 2%Ru-0.8%Re (Ru:Re = 9:2, Table 1). HAADF-STEM images (with good quality) and EDS spectra of a single nanoparticle in the 2%Ru-0.8%Re catalyst were unsuccessful since very small bimetallic NPs were found to be less stable under the electron beam (98% particles below 2 nm, Fig. 2). Release of atoms from the RuRe NPs during the analysis was observed, leading to the presence of defects on the outer shell of the nano-objects and isolated atoms on the grid. It could be noted that all prepared bimetallic nano-catalysts were highly dispersed, even those with high Ru and Re content, therefore we decided to perform STEM-HAADF characterization for sample with high Ru

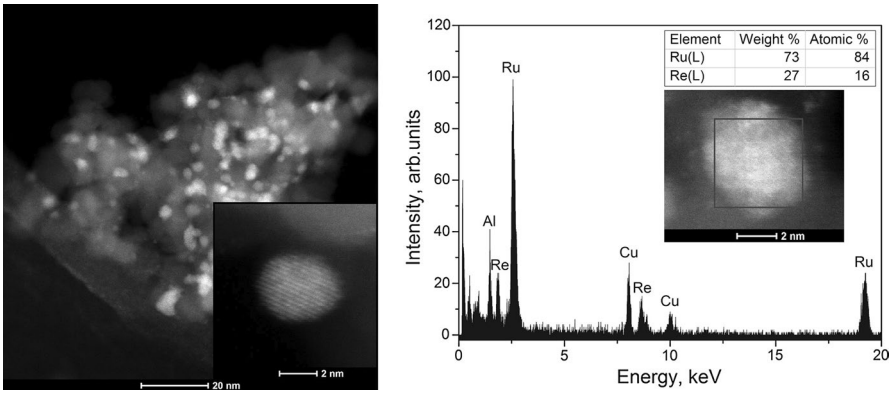

Fig. 3 Examples of the STEM-HAADF images obtained for the bimetallic 5%Ru-2%Re/γ-Al_2O_3 nano-catalyst treated in H_2 at 400 °C, and the corresponding EDS spectrum from the selected area

and Re content. The high magnification STEM-HAADF images of the 5%Ru-2%Re catalyst treated in hydrogen at 400 °C and corresponding lines in the EDS spectrum collected along active phase particles are shown in Fig. 3. The crystalline RuRe NPs with size of 1–4 nm are uniformly dispersed on the support, mostly as single particles. The presented EDS spectrum leads to the conclusion that small NPs consist of both Ru and Re atoms. Additionally, the Ru:Re atomic ratio in the analyzed particles (84:16) is very closed to the assumed one (90:20), taking into consideration the measurement error. The results evidence that the RuRe NPs with well-defined composition can be easily synthesized by the used colloidal method. Martynova et al. reported that ruthenium and rhenium can form bulk alloys with the composition of $Ru_{0.5}Re_{0.5}$ and $Ru_{0.67}Re_{0.33}$ [36].

Structure characterization of the nano-catalysts after air treatment at 500 °C

Before catalytic measurements the Ru and RuRe catalysts were heated in air at 500 °C, therefore we performed also structure characterization of the oxidized samples. Fig. 4 shows the XRD patterns recorded for the 2% Ru and all the bimetallic 2% Ru–Re nano-catalysts treated in air at 500 °C for 1 h. As can be seen, all the patterns show the characteristics reflections corresponding to RuO_2 in a tetragonal phase (JCPDS 40-1290), with (110), (101) and (211) as the prevailing primary orientations. For the 2% Ru nano-catalyst reflections from RuO_2 are narrow and intense and the mean crystallite size, calculated from the line broadening of the most intense peak at $2\theta = 28°$ is about 40 nm. Reflections of RuO_2 oxide are weaker and more broadened in the bimetallic Ru–Re nano-catalysts indicating that mean crystallite size of RuO_2 for these samples is smaller. As shown in Table 2, the crystallite size of RuO_2 is the smallest for the 2%Ru-0.8%Re nano-catalyst (20 nm) and at higher Re loadings a slight increase of the crystallite size of RuO_2 oxide is observed (maximum to 26 nm for 2%Ru-2%Re/γ-Al_2O_3). The XRD results evidently show that the presence of Re at loading of ≥ 0.8 wt% causes smaller aggregation of the Ru phase

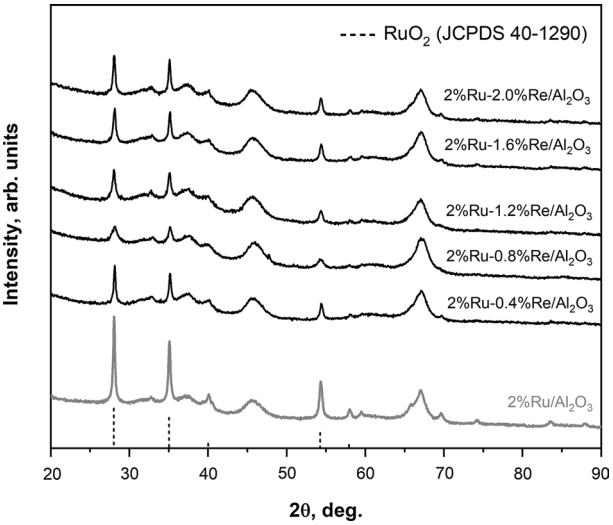

Fig. 4 X-ray diffraction patterns of the monometallic 2% Ru and bimetallic 2% Ru–Re/γ-Al_2O_3 nano-catalysts, after treatment in air at 500 °C for 1 h. All patterns show the characteristics reflections corresponding to RuO_2 (JCPDS 40-1290)

Table 2 The mean crystallite size of RuO_2 oxide after treatment of the nano-catalysts in air at 500 °C and after three cycles of soot combustion

Catalyst	RuO_2 crystallite size (nm)		BET surface area (m^2/g)	Mean pore diameter (nm)	Total pore volume (cm^3/g)
	Air, 500 °C	After soot combustion			
2% Ru	40	50	125	13.5	0.42
2%Ru-0.4%Re	35	40	126	16.9	0.55
2%Ru-0.8%Re	20	30	129	17.8	0.56
2%Ru-1.2%Re	24	35	124	16.8	0.55
2%Ru-1.6%Re Re	26	34	128	17.2	0.56
2%Ru-2.0%Re	26	35	127	17.1	0.57

Textural properties of the used samples i.e. after testing in three cycles of the catalytic soot combustion

in the bimetallic nano-catalysts during air oxidation at 500 °C. In the oxidized bimetallic Ru–Re samples no evidence of any rhenium oxide phase was found by XRD, although the ICP data confirmed that all Re was present in these nano-catalysts. Probably, rhenium oxide is present on the catalyst surface as highly dispersed ReO_x phase not giving detectable diffraction peaks.

We also performed characterization of the selected oxidized bimetallic Ru–Re samples by STEM-HAADF/EDS technique since this method is capable of providing simultaneous chemical and structural information with atomic resolution. As example, Fig. S1 (Supplementary Materials) shows representative high magnification STEM-HAADF image of the 2%Ru-0.8%Re/γ-Al_2O_3 nano-catalyst oxidized

at 500 °C and the EDS spectrum obtained from the selected area. Morphology of the oxidized nano-catalyst differs significantly from the morphology of the reduced bimetallic samples (Fig. 2B, C). Small, well-dispersed RuRe NPs are replaced with rather large (10–50 nm) RuO_2 crystallites, mainly in the shapes of elongated blocks. EDS analysis, conducted on the 2%Ru-0.8%Re sample, allowed us to examine how the chemical compositions of nano-catalysts changed after oxidation treatment. It is clearly visible that the EDS signal from the particle of Ru atoms is intensive, but Re atoms are not visible evidencing a separation between ruthenium and rhenium oxide phase. Nevertheless, after carefully measuring several particles with less defined shapes (Fig. S1), we were able to conclude, that the rhenium dopant was actually still there but its concentration in such large crystals was far from the assumed theoretical value. Since the concentration of Re in this sample is very low (~0.15 Re atoms/nm^2), determining the exact position of the oxidized ReO_x species was difficult. Using STEM-HAADF/EDS technique we previously evidenced for traditionally prepared bimetallic 5%Ru-3%Re/Al_2O_3 catalyst, aged in air at 500 °C for 3 h, that oxidized ReO_x species may be located both on the surface of larger RuO_2 oxide particles (as atomically dispersed species) and on the alumina support as very small clusters (~0.6 nm) [31]. Very recently, Ro et al. [37] found by using HAADF-STEM characterization the presence of dispersed co-localized atomically dispersed Rh and Re species in the Rh/ReO_x_Al_2O_3 catalysts after ex situ calcination at 350 °C. However, these catalysts were prepared by a special procedure i.e. via the targeted deposition of Rh precursors near atomically dispersed ReO_x on γ-Al_2O_3 using electrostatic interactions. In the HAADF-STEM images of the calcined monometallic ReO_x-Al_2O_3 samples atomically dispersed Re species but also Re clusters were observed [37]. These results are consistent with those presented earlier by Okal et al. who found that Re at low concentration on γ-Al_2O_3 support (0.2 Re/nm^2) after oxidation at 500–800 °C, is present as individual ReO_x species with an Al-O-ReO_3 structure [38] and at higher concentration (2.1 Re/nm^2) also as a surface compound exhibiting Al-(O-ReO_3)$_3$ structure [39].

XPS studies

The X-ray photoelectron spectroscopy (XPS) analysis revealed the oxidation states of the surface ruthenium and rhenium atoms in the selected Ru or Ru–Re nano-catalysts after heating in hydrogen at 400 °C and oxidation in air at 500 °C i.e. before activity measurements. The characterization of the Ru-based catalysts by this technique is difficult because Ru 3d spectra are severely overlapped with C 1 s peak (at 285.2–288 eV) of the various carbon bound species and also between the Re $4d_{3/2}$ and Ru $3d_{5/2}$ (major peaks). Large part of the carbon species may come from organic residues in agreement with literature data, which showed that at the surface of the Ru catalyst prepared by the polyol method, there is more C-containing species than at the surface of the traditional prepared catalyst (impregnation). Some part of the carbon residues was removed by heating of the as-prepared samples in hydrogen at 400 °C. A typical wide energy scans of the 2% Ru/γ-Al_2O_3 and 2%Ru-0.8%Re/γ-Al_2O_3 nan-catalyst after in situ treatment in hydrogen at 400 °C are shown in Supplementary Materials (Figs. S2 and

S3, respectively). The monometallic Ru sample gave an XPS spectrum with clearly resolved O 1 s and 2 s, Al 2 s and 2p, C 1 s, Ru 3p, Ru 3d peaks (Fig. S2) and for the bimetallic Ru–Re sample additionally Re 4d peak is also visible (Fig. S3). As an impurity only carbon (in four different states; C–H aliphatic, C–O, C=O and O–C=O) was observed in all the studied samples. It is important that chlorine ions were not present in the tested samples (Cl 2p peak at ~ 199 eV), although they were synthesized from Cl-containing Ru precursor ($RuCl_3$). Since $RuCl_3$ is often used in the preparation of the various Ru-based catalysts, it is available in the market and cheaper than other Ru precursors, thus the frequently observed the chlorine poisoning effect should be avoided, using the proposed microwave-polyol method to synthesize Ru–Re nano-catalysts.

Fig. S4 (Supplementary Materials) shows XPS high resolution spectra of the Ru 3d region from the 2% Ru catalyst and spectra of the Ru 3d and Re 4d regions from the bimetallic 2%Ru-0.8%Re/γ-Al_2O_3 after treatment with H_2 at 400 °C and after oxidation in air at 500 °C. More detailed deconvoluted high resolution spectra are also shown in Figs. S5 and S6. The XPS spectrum of the reduced Ru sample (Fig. S4a) shows two main components that contain $3d_{5/2}$ peak at ~ 279.7 eV, which is assigned to metallic Ru^0 species and at ~ 280.8 eV, which is attributed to Ru^{4+} species. After treatment in air at 500 °C, a strong peak at ~ 280.73 eV attributed to a $3d_{5/2}$ of Ru^{4+} species is observed (Fig. S4 b). Moreover, XPS spectra of the reduced and oxidized 2% Ru nano-catalyst contain also minor contributions from RuO_x surface species (at ~ 281.8 eV) and from satellite feature in RuO_2 (at ~ 282.6 eV). The XPS spectra of the reduced bimetallic 2%Ru-0.8%Re sample (Fig. S4 c) contain also metallic Ru^0 species (at ~ 279.8 eV) and Ru^{4+} species, and in the fully oxidized sample only Ru^{4+} species (at ~ 280.8 eV, Fig. S4 d). Additionally, in the reduced and oxidized Ru–Re catalyst (Fig. S4 c and d) spectra in the Re $4d_{3/2}$ region show only one low intense and broad peak and therefore determination of the rhenium oxidation states is impossible. Such large spectral broadening is also characteristic for the low-loaded Re/γ-Al_2O_3 catalysts and it is ascribed to the strong interaction of the rhenium species (mainly as ReO_x) with the alumina support [40]. In our case, we suppose that in the reduced Ru–Re/γ-Al_2O_3 sample significant amounts of Re species existed as a mixture of low-valent Re species (Re^{3+}, Re^{4+}, Re^{6+} and Re^{7+}) that may include also the metallic state. Previously, we found by XPS that in traditionally prepared 5%Ru-3%Re/γ-Al_2O_3 catalyst, after reduction in hydrogen at 500 °C, rhenium species existed as Re^0, Re^{4+}, Re^{6+} and Re^{7+} [28]. The presence of a mixture of various oxidation states is ascribed to the strong oxophilicity of rhenium [40]. We suppose that ReO_x oxide species in the reduced catalyst existed mainly on the surface of RuRe NPs in agreement with EDS results (Fig. 3), which showed that Ru and Re atoms were in close proximity. After oxidation at 500 °C, probably all Re species are oxidized to Re^{7+}, and large broadening of the Re XPS peak indicates that this species is present on the surface in various environments (Fig. S4 d).

Soot oxidation activity of Ru-based nano-catalysts in the presence of oxygen

The catalytic performance of the monometallic Ru and bimetallic RuRe/γ-Al_2O_3 nano-catalysts in the soot combustion was investigated by the thermogravimetric method using synthetic air atmosphere (21% O_2 and 79% N_2). Before measurements

the nano-catalysts were activated in air at 500 °C for 1 h. This activation resulted in a considerable reactivity for the catalytic soot oxidation and the commercially available soot, Printex80 from Degussa, is a good reference to the realistic particulate matters [41]. The results expressed as a soot conversion percentage as a function of temperature change for all studied samples are presented in Figs. 5 and S7. The scale was adjusted to present the obtained results the most accurately. Since the durability

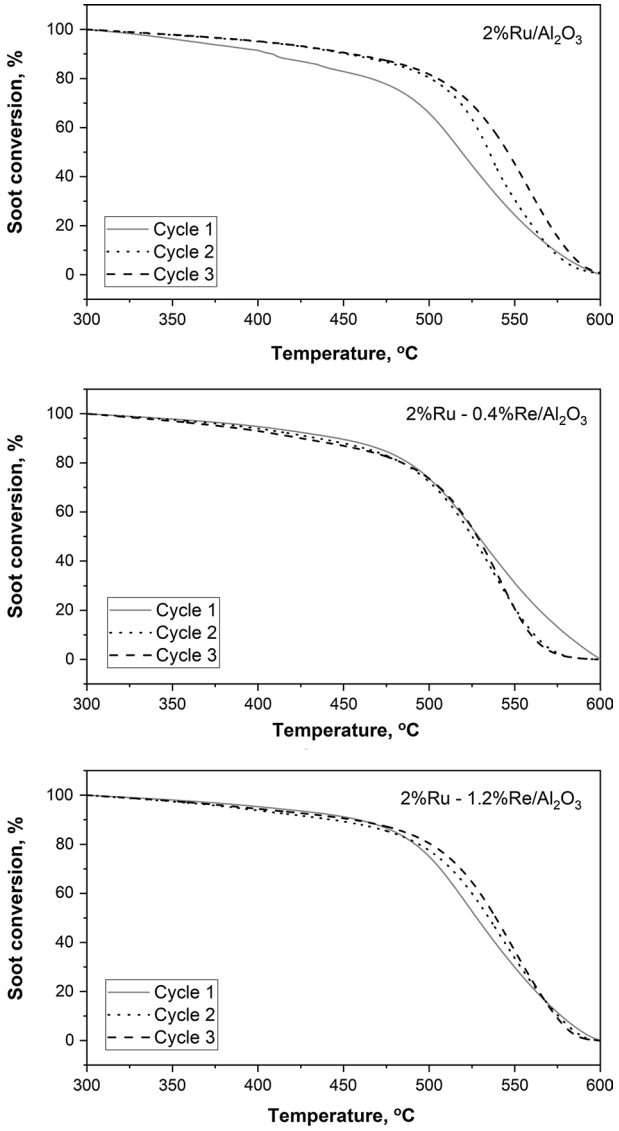

Fig. 5 Catalytic soot oxidation curves recorded during the three consecutive tests on the 2% Ru/γ-Al_2O_3, and bimetallic 2%Ru-0.4%Re and 2%Ru-1.2%Re nano-catalysts (soot:catalyst ratio = 1:8, in the flow of synthetic air 50 ml/min + Ar 20 ml/min)

of the catalysts is very necessary for their application, activity of the studied catalysts was evaluated in three consecutive cycle experiments. To compare the catalytic activities of the samples T_{10}, T_{50}, and T_{90} values (the temperature at which 10%, 50%, and 90% of the soot was oxidized, respectively) were chosen and are presented in Table 3. Additionally, catalytic properties of the studied catalysts were evaluated by comparing these temperatures with those of soot oxidation without any catalyst and over the monometallic Re/γ-Al_2O_3 catalyst in the same reaction conditions. As shown in Table 3, the temperature onset T_{10} for the non-catalytic soot oxidation is close to 465 °C, whereas nearly completed soot oxidation is observed at 670 °C. Similar the T_{10} and T_{90} values were obtained for soot oxidation over 0.8% Re/γ-Al_2O_3 catalyst. The results show that rhenium supported on γ-alumina is totally inactive in the soot oxidation. Literature data show that the non-catalytic combustion temperature of soot depends on the amount of adsorbed hydrocarbon molecules and experimental conditions, but generally is between 600 and 700 °C [9, 21, 42].

Fig. 5 shows the soot conversion over three representative catalysts, monometallic 2%Ru and bimetallic 2%Ru-0.4%Re and 2%Ru-1.2%Re, as a function of reaction temperature. In the first catalytic cycle the 2% Ru catalyst exhibited high activity. The onset of soot oxidation is observed at 403 °C, i.e. 62 °C below that of the uncatalyzed soot. After ignition, soot oxidation proceeds rapidly and the T_{90} value in the first cycle is close to 577 °C i.e. about 93 °C lower with respect to non-catalytic soot oxidation (Table 3). However, activity of this catalyst decreases quickly, already in the second measurement cycle (Fig. 5). Namely, the onset temperature (T_{10}) value

Table 3 T_{10}, T_{50}, T_{90} and ΔT for soot combustion in "tight contact" over the monometallic Re, Ru and bimetallic Ru–Re/γ-Al_2O_3 nano-catalysts prepared by the polyol method

Catalyst	Reaction cycle	T_{10} (°C)[a]	T_{50} (°C)[a]	T_{90} (°C)[a]	ΔT (°C)
Bare soot	1st	465	585	670	205
0.8%Re/γ-Al_2O_3	1st	462	578	668	206
2% Ru	1st	403	522	577	174
	2nd	448	535	578	130
	3rd	448	550	583	135
2%Ru-0.4%Re	1st	412	528	583	171
	2nd	430	525	557	122
	3rd	430	525	557	127
2%Ru-0.8%Re	1st	422	521	570	148
	2nd	420	525	568	148
	3rd	420	530	558	138
2%Ru-1.2%Re	1st	434	525	577	143
	2nd	431	532	575	144
	3rd	433	537	575	142
2%Ru-1.6%Re	1st	436	532	582	146
	2nd	440	534	576	136
	3rd	448	540	574	126
2%Ru-2%Re	1st	445	529	578	133
	2nd	446	536	574	128
	3rd	448	540	574	126

[a]The experimental error is ± 4 °C, for the tight contact in the soot:catalyst ratio used in this investigation

in the second and third cycle is about 45 °C higher (448 °C) as compared to the first cycle (403 °C). Also, the T_{50} value increased by about 13 °C in the second cycle and by 28 °C in the third cycle (550 °C, Table 3). For the bimetallic catalyst with small amount of Re (0.4 wt%) in the first catalytic cycle, the soot conversion curve shifts slightly towards the higher temperatures in comparison to the monometallic 2%Ru (Fig. 5, Table 3). However, the curves of the cycle experiments show a slight back shift compared to the catalytic curve of the fresh 2% Ru-0.4%Re catalyst, and the two curves almost overlap. Thus, in the second cycle, activity of this catalyst increased and the T_{90} value is about 26 °C lower (557 °C) as compared to the first cycle (583 °C) and in the third cycle the T_{10}, T_{50} and T_{90} values are the same as in the second cycle (Table 3). The best catalytic results, in terms of all the considered parameters, are observed when the Re content in the bimetallic sample was increased to 0.8 wt% (atomic ratio of Ru/Re is 9:2). As shown in Table 3, in the first catalytic cycle, the T_{50} and T_{90} values are close to that observed for the monometallic 2% Ru sample. However, in the second and third cycle these values are much lower, particularly the T_{90} value in the third cycle is observed near 558 °C, i.e. about 25 °C lower as compared to 2% Ru (583 °C) and about 112 °C below that of bare soot. Also, for this sample the T_{90} value in the third cycle is about 12 °C lower (558 °C) as compared to the first cycle (570 °C). A further increase in the rhenium content to 2 wt% (atomic ratio of Ru/Re is 9:5) leads to a small decrease in the catalyst activity in the first cycle (Figs. 5 and S7). However, as can be seen from Fig. S7 and Table 3, the T_{50} and T_{90} values in the second and third cycle are always lower for the bimetallic Ru–Re nano-catalysts as compared to the monometallic Ru nano-catalyst, independent of the Re content. It should be noted that the bimetallic Ru–Re/γ-Al_2O_3 nano-catalysts, with the Re loading of 0.4 and 0.8 wt%, have soot oxidation activity in the presence of oxygen very close to that reported for the Pt-K/Al_2O_3 catalyst [43], but slightly lower than for Ru supported on the reducible oxides (CeO_2, CeO_2–ZrO_2), for which the presence of Ru–O–Ce species is favorable for this reaction [20, 21, 42–44]. Querini et al. [45, 46] studied the catalytic combustion of diesel soot using Co/MgO, K/MgO and Co–K/MgO catalysts, which are much cheaper than those used in this study. The authors reported negligible activities for pure MgO and K/MgO. For the Co/MgO catalysts, a direct relation between catalytic activity and cobalt reducibility was found, suggesting that the reaction proceeds through a redox mechanism. This catalyst burns out the soot between 450 and 550 °C depending on the calcination temperature, but the Co/MgO sample calcined at 500 °C or higher was inactive, and the formation of the solid solution Co ± Mg was responsible for the loss of activity [45]. Catalytic activity of the Co/MgO calcined at 400 °C increased with the addition of potassium and there was an optimum in the potassium content. The Co–K/MgO catalyst containing 4.5% of K presented a temperature of maximum combustion rate at 378 °C, whereas those containing 1.5% and 7.5% of K at temperatures over 400 °C [46]. On the other hand, Jiménez et al. [47] found that calcination of the K/MgO catalyst at 760 °C, instead 400 °C as was applied by Querini et al., cause significant increase its activity (T_{10} = 399 °C T_{max} = 440 °C, "tight" contact with carbon black). It could be noted however, that comparing the catalytic performances of our Ru-based nano-catalysts is difficult since activity of various soot combustion catalysts depends on many factors such as

the soot-catalyst ratio, the type of catalyst-soot contact, the soot composition and the content of oxygen in the feed mixture, and a great variation of these parameters can be found in the literature [4].

It is worth to note that the onset combustion temperature, defined as the temperature at which 10% of the soot is converted, was also considered in order to better discriminate the intristic catalytic activity of the synthesized mono- and bimetallic Ru–Re nano-catalysts. The tight contact maximizes the soot contact with the catalyst, thus the onset combustion temperature depends only on the catalytic reaction, in a reaction rate limited regime. At higher soot conversion degrees, other phenomena such as mass transfer or hot spots could influence the real hierarchy of the catalysts. As shown in Table 3, in the first catalytic cycle, the onset of soot oxidation is the lowest for the monometallic 2% Ru nano-catalyst (403 °C) and T_{10} successively increases for the bimetallic Ru–Re nano-catalysts from 412 to 445 °C when the Re content increases from 0.4 to 2 wt%. Because rhenium alone is not active in the soot combustion reaction (Table 3), we suppose that some covering of the active Ru phase by the ReO_x species could lower the intristic catalytic activity of the Ru phase. HAADF-STEM characterization demonstrated that Re species may be located both on the alumina surface and on the surface of RuO_2 oxide particles. On the other hand, for the bimetallic catalysts containing 0.8–2 wt% of Re, during the whole cycle experiment ΔT does not change much in the three reaction cycles, which indicates that these samples have high and stable catalytic activity for soot combustion. For the 2% Ru and 2% Ru-0.4%Re nano-catalysts, ΔT in the first reaction cycle is similar (174–171 °C, Table 3) and it is much higher than in the next catalytic cycles, which may be due to the structural changes as the cycle experiment progresses, which are crucial for maintaining the satisfactory catalytic activity. Probably the Re content is insufficient to obtain a stable bimetallic nano-catalyst when the atomic ratio of Ru/Re is equal to 9:1 (Table 1). Therefore, the activity results indicate that although monometallic 2% Ru nano-catalyst exhibited the highest intristic activity however, bimetallic Ru–Re/Al_2O_3 samples are much more stable during the whole catalytic experiment. The activity of the Ru–Re catalysts basically does not change in the second and third catalytic cycles. Villani et al. [23] reported that the carbon oxidation activity of Ru/Na-Y is related to the Ru content and the T_{10} values at Ru loadings of 0.3, 3 and 7.5% were 396, 373 and 356 °C, respectively. The Ru/Al_2O_3 was less active and the observed T_{10} value was found to be 415 °C [23] i.e. at higher temperature than that found for our monometallic 2% Ru nano-catalyst (T_{10} = 403 °C).

To better analyze the change of the catalytic activity of the catalysts in the soot oxidation we took into consideration: (a) changes of the specific BET surface area, (b) possible loss of the Re and Ru oxides by volatilization during heating under soot/oxygen mixture at high temperature (up to 600 °C), and (c) changes in the catalyst structure. Thus, the Ru-based catalysts after testing in three cycles were characterized by N_2 adsorption–desorption measurements, ICP-AES and XRD methods. As shown in Table 2, all used nano-catalysts have similar BET surface areas (124–129 m^2/g) and are only slightly lower than the fresh air treated catalysts (134–138 m^2/g, Table 1). However, the mean pore diameter and total pore volume of the used 2% Ru/γ-Al_2O_3 (13.5 nm and 0.42 cm^3/g, respectively) are much lower than

in the used bimetallic Ru–Re/γ-Al_2O_3 catalysts (16.8–17.8 nm and 0.55–0.57 cm^3/g, respectively) and lower than in all catalysts before catalytic measurements (18.1–19 nm, and 0.62–0.65 cm^3/g, respectively, Table 1). Therefore, the observed some deactivation of the 2% Ru nano-catalyst may be caused by the changes in the support structure, i.e. pore blockage by the larger RuO_2 oxide particles formed during the course of the catalytic reaction. ICP-AES measurements of the 2% Ru and selected two bimetallic Ru–Re samples confirm that Ru and Re contents in the used catalysts are close to that in the fresh samples (Table S1, Supplementary Materials) evidencing that no loss of Ru or Re as volatile RuO_4 or Re_2O_7 oxide occurs during the soot combustion up to 600 °C. Strong interaction of the oxidized Re species with γ-Al_2O_3, especially large at low loading, prevented its loss from the catalysts surface even at high temperature [39, 40]. Aouad et al. reported for the supported Ru-based catalysts, used in propene and carbon black oxidation, that above 730 °C RuO_2 is oxidized and forms volatile RuO_4 oxide and this results in Ru loss [42]. In our study complete combustion of soot occurs at lower temperatures (< 583 °C, Table 3) and therefore, loss of Ru and Re was prevented.

Structure characterization of the used catalysts by XRD show that all the Ru and bimetallic Ru–Re nano-catalysts exhibited the XRD patterns with the diffraction peaks of RuO_2 oxide. The XRD patterns, shown in the Supplementary Materials (Fig. S8) are similar to those obtained after oxidation treatment at 500 °C i.e. as before catalytic measurements (Fig. 4). Diffraction peaks of the RuO_2 oxide are basically very similar for all used Ru–Re/Al_2O_3 samples, but more intense in the case of the 2% Ru nano-catalyst, indicating that monometallic Ru catalyst exhibits a sintering phenomenon. The mean crystallite size of RuO_2 is 50 nm for the used 2% Ru i.e. higher than that before catalytic experiments (40 nm, Table 2). For the used bimetallic Ru–Re samples, with Re content ≥ 0.8 wt%, the crystallite size of RuO_2 is much lower (30–36 nm, Table 2). These data are in good agreement with the activity results (Table 3), which show that all the Ru–Re nano-catalysts in the 3rd cycle exhibited higher overall catalytic performance as compared to that of the 2% Ru nano-catalyst.

Summarizing, the characterization data of the used samples clearly indicate that deactivation of the monometallic Ru nano-catalyst, due to nanoparticle sintering, is significantly greater than that of the bimetallic Ru–Re nano-catalysts. Therefore, the presence of rhenium in the catalytic system hinder the formation of large RuO_2 agglomerates leading to a better dispersion of the ruthenium phase and therefore a better catalytic performance of Ru–Re nano-catalysts. Also, in the traditionally prepared 5% Ru–Re catalysts, containing 1 or 3 wt% of Re, the suppress RuO_2 particles sintering was observed during propane combustion reaction [28]. It is well known that the reaction of soot combustion is a redox process, in which the soot acts as a reducing agent during the reaction. Our XPS studies of Ru and Ru–Re nano-catalysts showed that different reactive ruthenium oxide species are formed following air treatment at 500 °C (Fig. S4). The ability of RuO_2 particles or RuO_x species to undergo redox cycles required for oxidation reactions is well known [15, 28] Thus, we suppose that lattice oxygen atoms from small RuO_2 particles or partially oxidized RuO_x forms can be available for soot combustion reaction. The higher concentration of the smaller RuO_2 crystallites in the bimetallic Ru–Re nano-catalysts, in

comparison to the monometallic Ru, leads to the higher activity of this system in the catalytic soot combustion. Literature data and our previously reported volumetric O_2 adsorption results for the 5% Ru and 5% Ru–Re catalysts revealed also that some weak dissociative oxygen adsorption take place on the surface of the RuO_2 particles [28, 48]. It is known that the stoichiometric RuO_2(110) surface exposes coordinatively unsaturated (cus) Ru atoms onto which dissociative adsorption of oxygen (O-cus) may occur [14]. Dissociative adsorption of oxygen on Ru sites followed by its reaction with the solid carbon at the soot-catalyst interface could be also a possible mechanism for soot combustion over the Ru-based nano-catalysts. Additionally, some literature results reported that ReO_x clusters can play significant role in the activation of oxygen to produce oxidizing species in the case of Pt-ReO_x/SiO_2 catalyst [49]. Finally, under oxidizing conditions and temperatures above 400 °C, some loss of the activity of the ruthenium catalysts may be correlated with the transformation of the catalytically active RuO_2(100) phase into a reconstructed c(2 × 2) domains [50]. It is possible that rhenium presence in the Ru–Re nano-catalysts may inhibit the RuO_2(100) growth on the surface of the small RuO_2 crystallites and its transformation into inactive c(2 × 2) surface facets.

Conclusion

A series of bimetallic Ru–Re/Al_2O_3 nano-catalysts with different atomic ratios (Ru/Re = 9:1, 9:2, 9:3, 9:4 and 9:5) were synthesized by the microwave polyol method and their activity in model soot oxidation was investigated (tight contact, in the absence of NO_x). In the first catalytic cycle the temperature of soot ignition for Ru nano-catalyst was found at 403 °C, while for Ru–Re nano-catalysts it was found to be in the range of 412- 445 °C. However, in the next catalytic cycles, bimetallic catalysts were more active than monometallic Ru sample. The presence of Re in the bimetallic Ru–Re/Al_2O_3 nano-catalysts prevents the growth of RuO_2 crystallites, which in turn leads to greater activity and stability of these nano-catalysts, regardless of the Re amount. The activity of soot oxidation over Ru–Re nano-catalysts depended on the amount of Re and the highest catalytic performance exhibited the 2% Ru-0.8%Re nano-catalyst with atomic ratio Ru/Re = 9:2. When the rhenium amount was too high (≥ 1.6 wt%), the activity of the catalytic system slightly decreased, probably because of the Ru surface blockage by an inactive oxidized ReO_x species.

Combining the facts that we proved previously Ru–Re catalysts are active and stable in oxidation of volatile organic compounds and we now showed they can be also stable and active in the catalytic soot combustion, bimetallic Ru–Re nano-catalysts prepared by polyol methods, can be a good alternative for Pt or Pd catalysts for particle matters oxidation.

Supplementary Information The online version contains supplementary material available at https://doi.org/10.1007/s11144-021-02048-y.

Acknowledgements The authors wish to thank: Mrs. Ewa Bukowska for the XRD measurements, Mrs. Dagmara Białowieska, Mrs. Patrycja Kokot vel Kokocińska and Agnieszka Siomra for technical

assistance and Dr. Marcin Kuśmierz for the XPS studies. This work was carried out within the Reintegration programme of the Foundation for Polish Science co-financed by the European Union under the European Regional Development Fund, project no. POIR.04.04.00-00-5F33/18-00.

Author contributions KA: methodology, visualization, investigation, formal analysis, funding acquisition, writing—original draft, SS: investigation, methodology, formal analysis, writing, SZ: methodology, investigation, DS: methodology, investigation, AH: methodology, investigation, PS: methodology, writing—review and editing, AK: conceptualization, supervision, writing—review, JO: conceptualization, writing—review and editing. All authors have read and agreed to the published version of the manuscript.

Declarations

Conflict of interest The authors declare that they have no conflict of interest concerning this article.

References

1. Mamakos A, Martini G, Marotta A, Manfredi U (2013) Assessment of different technical options in reducing particle emissions from gasoline direct injection vehicles. J Aerosol Sci. https://doi.org/10.1016/j.jaerosci.2013.05.004
2. Li N, Xia T, Nel AE (2008) The role of oxidative stress in ambient particulate matter-induced lung diseases and its implications in the toxicity of engineered nanoparticles. Free Radic Biol Med. https://doi.org/10.1016/j.freeradbiomed.2008.01.028
3. Prasad R, Bella VR (2010) A review on diesel soot emission, its effect and control. Bull Chem React Eng Catal. https://doi.org/10.9767/bcrec.5.2.794.69-86
4. Fino D, Bensaid S, Piumetti M, Russo N (2016) A review on the catalytic combustion of soot in diesel particulate filters for automotive applications: from powder catalysts to structured reactors. Appl Catal A: Gen. https://doi.org/10.1016/j.apcata.2015.10.016
5. Guan B, Zhan R, Lin H, Huang Z (2015) Review of the state-of-the-art of exhaust particulate filter technology in internal combustion engines. J Environ Manag. https://doi.org/10.1016/j.jenvman.2015.02.027
6. Burch R (2004) Knowledge and know-how in emission control for mobile applications. Catal Rev-Sci Eng. https://doi.org/10.1081/CR-200036718
7. Bueno-López A (2014) Diesel soot combustion ceria catalysts. Appl Catal B: Environ. https://doi.org/10.1016/j.apcatb.2013.02.033
8. Gandhi HS, Graham GW, McCabe RW (2003) Automotive exhaust catalysis. J Catal. https://doi.org/10.1016/S0021-9517(02)00067-2
9. Ramdas R, Nowicka E, Jenkins R, Sellick D, Davies C, Golunski S (2015) Using real particulate matter to evaluate combustion catalysts for direct regeneration of diesel soot filters. Appl Catal B: Environ. https://doi.org/10.1016/j.apcatb.2015.04.031
10. Kittelson DB (1998) Engines and nanoparticles: a review. J Aerosol Sci. https://doi.org/10.1016/S0021-8502(97)10037-4

11. Totton TS, Misquitta AJ, Kraft M (2012) A quantitative study of the clustering of polycyclic aromatic hydrocarbons at high temperatures. Phys Chem Chem Phys. https://doi.org/10.1039/C2CP23008A
12. Raróg-Pilecka W, Miśkiewicz E, Szmigiel D, Kowalczyk Z (2005) Structure sensitivity of ammonia synthesis over promoted ruthenium catalysts supported on graphitised carbon. J Catal. https://doi.org/10.1016/j.jcat.2004.12.005
13. King DL (1978) A Fischer-Tropsch study of supported ruthenium catalysts. J Catal. https://doi.org/10.1016/0021-9517(78)90277-4
14. Wang Y, Jacobi K, Schöne WD, Ertl G (2005) Catalytic oxidation of ammonia on RuO_2(110) surfaces: mechanism and selectivity. J Phys Chem B. https://doi.org/10.1021/jp045735v
15. Liu H, Iglesia E (2005) Selective oxidation of methanol and ethanol on supported ruthenium oxide clusters at low temperatures. J Phys Chem B. https://doi.org/10.1021/jp0401980
16. Blume R, Hävecker M, Zafeiratos S, Teschner D, Kleimenov E, Knop-Gericke A, Schlögl R, Barinov A, Dudin P, Kiskinova M (2006) Catalytically active states of Ru(0001) catalyst in CO oxidation reaction. J Catal. https://doi.org/10.1016/j.jcat.2006.02.019
17. Zhang XW, Shen SC, Yu LE, Kawi S, Hidajat K, Simon Ng KY (2003) Oxidative decomposition of naphthalene by supported metal catalysts. Appl Catal A: Gen. https://doi.org/10.1016/S0926-860X(03)00412-5
18. Okal J, Zawadzki M, Tylus W (2011) Microstructure characterization and propane oxidation over supported Ru nanoparticles synthesized by the microwave-polyol method. Appl Catal B: Environ. https://doi.org/10.1016/j.apcatb.2010.10.028
19. Okal J, Zawadzki M, Kraszkiewicz P, Adamska K (2018) Ru/CeO_2 catalysts for combustion of mixture of light hydrocarbons: effect of preparation method and metal salt precursors. Appl Catal A: Gen. https://doi.org/10.1016/j.apcata.2017.09.036
20. Aouad S, Abi-Aad E, Aboukaïs A (2009) Simultaneous oxidation of carbon black and volatile organic compounds over Ru/CeO_2 catalysts. Appl Catal B: Environ. https://doi.org/10.1016/j.apcatb.2008.10.002
21. Homsi D, Aouad S, El Nakat J, El Khoury B, Obeid P, Abi-Aad E, Aboukaïs A (2011) Carbon black and propylene oxidation over $Ru/Ce_xZr_{1-x}O_2$ catalysts. Catal Commun. https://doi.org/10.1016/j.catcom.2011.01.014
22. Tschamber V, Jeguirim M, Villani K, Martens JA, Ehrburger P (2007) Comparison of the activity of Ru and Pt catalysts for the oxidation of carbon by NO_2. Appl Catal B: Environ. https://doi.org/10.1016/j.apcatb.2006.10.016
23. Villani K, Kirschhock CEA, Liang D, Van Tendeloo G, Martens JA (2006) Catalytic carbon oxidation over ruthenium-based catalysts. Angew Chem. https://doi.org/10.1002/anie.200503799
24. Jeguirim M, Villani K, Brilhac JF, Martens JA (2010) Ruthenium and platinum catalyzed carbon oxidation: a comparative kinetic study. Appl Catal B:Environ. https://doi.org/10.1016/j.apcatb.2010.01.031
25. Perkas N, Zhong Z, Chen L, Besson M, Gedanken A (2005) Sonochemically prepared high dispersed Ru/TiO_2 mesoporous catalyst for partial oxidation of methane to syngas. Catal Lett. https://doi.org/10.1007/s10562-005-6496-4
26. Baranowska K, Okal J, Tylus W (2016) Microwave-assisted polyol synthesis of bimetallic RuRe nanoparticles stabilized by PVP or oxide supports (γ-alumina and silica). Appl Catal A: Gen. https://doi.org/10.1016/j.apcata.2015.11.045
27. Baranowska K, Okal J (2017) Microwave assisted polyol synthesis of the bimetallic RuRe nanoparticles deposited on γ-alumina and their application for the light alkane oxidation. Top Catal. https://doi.org/10.1007/s11244-016-0610-2
28. Baranowska K, Okal J (2015) Bimetallic $Ru-Re/\gamma-Al_2O_3$ catalysts for the catalytic combustion of propane: effect of the Re addition. Appl Catal A: Gen. https://doi.org/10.1016/j.apcata.2015.04.023
29. Baranowska K, Okal J, Miniajluk N (2014) Effect of rhenium on ruthenium dispersion in the $Ru–Re/\gamma-Al_2O_3$ catalysts. Catal Lett. https://doi.org/10.1007/s10562-013-1169-1
30. Kluksdahl HE (1968) Reforming a sulfur-free naphtha with a platinum-rhenium catalyst, US Patent 3415737
31. Okal J, Zawadzki M, Baranowska K (2016) Methane combustion over bimetallic $Ru-Re/\gamma-Al_2O_3$ catalysts: effect of Re and pretreatments. Appl Catal B: Environ. https://doi.org/10.1016/j.apcatb.2016.04.038
32. Di X, Li C, Zhang B, Qi J, Li W, Su D, Liang C (2017) Role of Re and Ru in Re-Ru/C bimetallic catalysts for the aqueous hydrogenation of succinic acid. Ind Eng Chem Res. https://doi.org/10.1021/acs.iecr.6b04875

33. Bin Jung K, Lee J, Ha JM, Lee H, Suh DJ, Jun CH, Jae J (2018) Effective hydrodeoxygenation of lignin-derived phenols using bimetallic RuRe catalysts: effect of carbon supports. Catal Today. https://doi.org/10.1016/j.cattod.2017.07.027
34. Kim M, Ha JM, Lee KY, Jae J (2016) Catalytic transfer hydrogenation/hydrogenolysis of guaiacol to cyclohexane over bimetallic RuRe/C catalysts. Catal Commun. https://doi.org/10.1016/j.catcom.2016.08.022
35. Jin X, Thapa PS, Subramaniam B, Chaudhari RV (2016) Kinetic modeling of sorbitol hydrogenolysis over bimetallic RuRe/C catalyst. ACS Sustain Chem Eng. https://doi.org/10.1021/acssuschemeng.6b01346
36. Martynova SA, Yusenko KV, Korolkov IV, Baidina IA, Korenev SV (2009) X-ray diffraction study of $[Ru(NH_3)_5Cl][ReCl_6]$ and $[Ru(NH_3)_5Cl]_2[ReCl_6]Cl_2$ and their thermolysis products. Crystal-chemical analysis of the Ru–Re system. J Struct Chem. https://doi.org/10.1007/s10947-009-0016-0
37. Ro I, Xu M, Graham GW, Pan X, Christopher P (2019) Synthesis of heteroatom Rh−ReOx atomically dispersed species on Al_2O_3 and their tunable catalytic reactivity in ethylene hydroformylation. ACS Catal. https://doi.org/10.1021/acscatal.9b02111
38. Okal J, Kępiński L, Krajczyk L, Tylus W (2003) Oxidation and redispersion of a low-loaded Re/γ-Al_2O_3 catalyst. J Catal. https://doi.org/10.1016/S0021-9517(03)00165-9
39. Okal J, Kępiński L, Krajczyk L, Drozd M (1999) Oxidation and redispersion of a Re/γ-Al_2O_3 catalyst. J Catal. https://doi.org/10.1006/jcat.1999.2634
40. Okal J, Tylus W, Kępiński L (2004) XPS study of oxidation of rhenium metal on γ-Al_2O_3 support. J Catal. https://doi.org/10.1016/j.jcat.2004.05.004
41. Stanmore BR, Brilhac JF, Gilot P (2001) The oxidation of soot: a review of experiments, mechanisms and models. Carbon. https://doi.org/10.1016/S0008-6223(01)00109-9
42. Aouad S, Saab E, Abi Aad E, Aboukais A (2007) Reactivity of Ru-based catalysts in the oxidation of propene and carbon black. Catal Today. https://doi.org/10.1016/j.cattod.2006.08.030
43. Matarrese R, Morandi S, Castoldi L, Villa P, Lietti L (2017) Removal of NOx and soot over Ce/Zr/K/Me (Me = Fe, Pt, Ru, Au) oxide catalysts. Appl Catal B: Environ. https://doi.org/10.1016/j.apcatb.2016.07.013
44. Kurnatowska M, Mista W, Mazur P, Kepinski L (2014) Nanocrystalline Ce1-xRuxO2—microstructure, stability and activity in CO and soot oxidation. Appl Catal B: Environ. https://doi.org/10.1016/j.apcatb.2013.10.047
45. Querini CA, Ulla MA, Requejo F, Soria J, Sedrán UA, Miró EE (1998) Catalytic combustion of diesel soot particles. Activity and characterization of Co/MgO and Co,K/MgO catalysts. Appl Catal B: Environ. https://doi.org/10.1016/S0926-3373(97)00032-5
46. Querini CA, Cornaglia LM, Ulla MA, Miró EE (1999) Catalytic combustion of diesel soot on Co K/MgO catalysts. Effect of the potassium loading on activity and stability. Appl Catal B: Environ. https://doi.org/10.1016/S0926-3373(98)00109-X
47. Jiménez R, García X, Cellier C, Ruiz P, Gordon AL (2006) Soot combustion with K/MgO as catalyst. Appl Catal A: Gen. https://doi.org/10.1016/j.apcata.2005.08.042
48. Kim YD, Seitsonen AP, Wendt S, Wang J, Fan C, Jacobi K, Over H, Ertl G (2001) Characterization of various oxygen species on an oxide surface: RuO2(110). J Phys Chem B. https://doi.org/10.1021/jp003213j
49. Ebashi T, Ishida Y, Nakagawa Y, Ito S, Kubota T, Tomishige K (2010) Preferential CO oxidation in a H-2-rich stream on Pt-ReOx/SiO_2 catalyst structure and reaction mechanism. J Phys Chem C. https://doi.org/10.1021/jp911908c
50. Aßmann J, Crihan D, Knapp M, Lundgren E, Löffler E, Muhler M, Narkhede V, Over H, Schmid M, Seitsonen AP, Varga P (2005) Understanding the structural deactivation of ruthenium catalysts on an atomic scale under both oxidizing and reducing conditions. Angew Chem. https://doi.org/10.1002/anie.200461805